Anisotropic-vortex-flux production and retention in grain-oriented $YBa_2Cu_3O_7$

Liwen Liu and J. S. Kouvel
Department of Physics, University of Illinois at Chicago, Chicago, Illinois 60680

T. O. Brun
Los Alamos National Laboratory, Los Alamos, New Mexico 87545

(Received 9 August 1991)

Magnetization-vector measurements were made on a zero-field-cooled sample at 4.2 K in an increasing magnetic field (**H**) oriented at various angles (θ_H) relative to the *a-b* plane, with **H** corrected for demagnetization. For H above H_{c1}, it is found that $\mathbf{M}_P$, the penetrating vortex-flux component of the sample magnetization, forms first at angles (θ_P) relative to *a-b* that are generally much smaller than θ_H. The preference of the initial $\mathbf{M}_P$ for the *a-b* plane contrasts with the remanent trapped-flux magnetization $\mathbf{M}_R$, which is oriented preferentially toward the *c* axis. Nevertheless, both phenomena are qualitatively consistent regarding the strong anisotropy of the vortex-pinning forces in this layered crystal structure. Furthermore, it is found that for all θ_H the components of $\mathbf{M}_P$ along *a-b* and *c* versus the corresponding components of **H** describe two independent universal curves, suggesting that the vortices produced by **H** after zero-field cooling may lie only along *a-b* and/or along *c*. However, the results for $\mathbf{M}_R$ do not obey an analogous scaling and suggest that the path of the trapped vortices may alternate stepwise between *a-b* and *c*.

INTRODUCTION

The crystallographic asymmetry of the CuO_2-layered superconducting compounds is clearly reflected in the anisotropic character of the vortex state. As predicted theoretically[1] and observed directly in a $YBa_2Cu_3O_7$ crystal,[2] the vortex lines aligned in the *a-b* plane are very different in morphology from those aligned along the *c* axis. Relatedly, the same experiments[2] indicated that the vortex pinning may also in part be intrinsic to the crystal structure, as was also anticipated theoretically.[1,3] Relevant to this point, magnetic measurements on field-cooled crystals of $YBa_2Cu_3O_7$ and $Bi_2Sr_2CaCu_2O_8$ have revealed[4] that for different directions of the field applied during cooling, the trapped flux (in zero field) is oriented closely parallel to the *c* axis, implying that the pinning is strongest by far for the vortex lines along *c*.

The latter results raise the interesting related question as to the orientation of the vortex flux produced, after zero-field cooling, by fields (**H**) of different directions and of magnitudes exceeding the lower critical field H_{c1}. The experiments that can address this question would require that the sample magnetization be measured as a vector (**M**) relative to **H** and that the vortex-flux component of **M** be separated from the diamagnetic (screening) component. We have carried out such magnetization-vector measurements on a zero-field cooled grain-oriented sample of $YBa_2Cu_3O_7$ at 4.2 K in an increasing **H** of various directions, and we have decomposed the measured **M** into the appropriate components. Our findings for the field-induced vortex flux and those for the trapped flux (after the field is subsequently removed), which are reported here, are broadly consistent about the anisotropy of the vortex pinning forces but, in detail, imply that the vortex lines in the two states may be quite different in the nature of their paths.

EXPERIMENTAL PROCEDURE

In our experiments the sample was a circular disk (5-mm diam, 1-mm thick) cut from a boule prepared at the Los Alamos National Laboratory, in which small crystallites of $YBa_2Cu_3O_7$ in an epoxy matrix had been field oriented such that their *c* axes are coaligned, with the *a* and *b* axes randomly directed in the basal plane. The collective *c* axis lay in the plane of the sample disk, within which an external magnetic field $\mathbf{H}_e$ was applied in various directions. Simultaneous measurements were made of M_L and M_T, the longitudinal and transverse components of the magnetization vector **M** relative to $\mathbf{H}_e$, by means of a vibrating-sample magnetometer with two sets of pickup coils mounted in quadrature.

The experimental situation is represented schematically in the vector diagram of Fig. 1, which also shows M_{ab} and M_c, the components of **M** in the *a-b* plane and along the *c* axis. Associated with these are the corresponding components of a demagnetizing field, $H_d^{(ab)} = -D_{ab}M_{ab}$ and $H_d^{(c)} = -D_c M_c$, where we assume that all the crystallites are approximately spheroidal in shape with their axes of rotation parallel to *c*, such that $2D_{ab} + D_c = 4\pi$. To determine D_{ab} and D_c we measured the magnetization curves after zero-field cooling to 4.2 K and then applying $\mathbf{H}_e$ along *a-b* or along *c*, for which the initial linear variations of M_{ab} and M_c with H_e (below H_{c1}) may be expressed as

$$M_{ab} = -\chi_0 H_e^{(ab)}/(1-\chi_0 D_{ab}) \quad (1a)$$

and

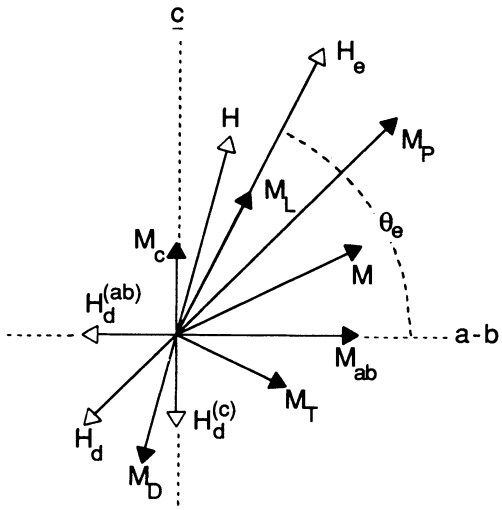

FIG. 1. Schematic vector diagram showing sample magnetization $\mathbf{M}$ and its measured longitudinal and transverse components $(\mathbf{M}_L,\mathbf{M}_T)$ relative to external field $\mathbf{H}_e$ at angle θ_e relative to *a-b* plane. Also shown are the components of $\mathbf{M}$ and of demagnetization field $\mathbf{H}_d$ along *a-b* and *c*, the internal field $\mathbf{H}$ $(=\mathbf{H}_e+\mathbf{H}_d)$, the diamagnetic screening magnetization $\mathbf{M}_D$ $(=-\mathbf{H}/4\pi)$, and the penetrating vortex-flux magnetization $\mathbf{M}_P$ $(=\mathbf{M}-\mathbf{M}_D)$.

$$M_c=-\chi_0 H_e^{(c)}/(1-\chi_0 D_c) , \tag{1b}$$

where χ_0 is the magnitude of the diamagnetic screening susceptibility. Assuming that the screening for the crystallites in our sample is essentially perfect, such that $\chi_0=1/4\pi$, we used these equations to obtain a normalization of the measured M_{ab} and M_c to the volume of the crystallites as well as to evaluate the interrelated D_{ab} and D_c. In this way we found that the volume fraction of the $YBa_2Cu_3O_7$ crystallites in our bulk sample is 0.049, indicating that they are dispersed dilutely in the epoxy matrix. We also found that $D_{ab}=3.364$ and $D_c=5.838$, which imply that the spheroidal shape assumed for the crystallites is distinctly oblate.

This numerical information enabled us to reduce and analyze our data for M_L and M_T versus H_e for different directions of $\mathbf{H}_e$. First, with reference to Fig. 1, the components of the demagnetization-corrected field $\mathbf{H}$ $(=\mathbf{H}_e+\mathbf{H}_d)$ along *a-b* and along *c* are as follows:

$$H_{ab}=(H_e-D_{ab}M_L)\cos\theta_e-D_{ab}M_T\sin\theta_e \tag{2a}$$

and

$$H_c=(H_e-D_cM_L)\sin\theta_e+D_cM_T\cos\theta_e , \tag{2b}$$

where θ_e is the angle between $\mathbf{H}_e$ and the *a-b* plane. Second, we decomposed the total measured $\mathbf{M}$ vector into the sum of a penetrating vortex-flux component $\mathbf{M}_P$ and a diamagnetic screening component $\mathbf{M}_D$. Regarding the latter, rotational measurements of $\mathbf{M}$, similar to those we performed earlier on polycrystalline Nb (Ref. 5) and $YBa_2Cu_3O_7$ (Ref. 6), revealed analogously that $\mathbf{M}_D$ closely equals $-\chi_0\mathbf{H}$ (with χ_0 taken to be $1/4\pi$) for $\mathbf{H}$ along *a-b* or *c* even when its magnitude far exceeds H_{c1}. We therefore considered for our grain-oriented sample that $\mathbf{M}_D=-\mathbf{H}/4\pi$ is valid isotropically up to our highest fields of measurement. Hence, consistent with Eq. (2), the components of $\mathbf{M}_P$ $(=\mathbf{M}-\mathbf{M}_D)$ along *a-b* and *c* may be expressed as

$$M_P^{(ab)}=[\chi_0H_e+(1-\chi_0D_{ab})M_L]\cos\theta_e +(1-\chi_0D_{ab})M_T\sin\theta_e \tag{3a}$$

and

$$M_P^{(c)}=[\chi_0H_e+(1-\chi_0D_c)M_L]\sin\theta_e -(1-\chi_0D_c)M_T\cos\theta_e , \tag{3b}$$

with $\chi_0=1/4\pi$. In summary, as represented in Fig. 1, Eqs. (2) and (3) give the components of $\mathbf{H}$ and $\mathbf{M}_P$ in terms of the measured M_L and M_T and the experimental variables H_e and θ_e.

RESULTS AND DISCUSSION

Our experiments were all carried out after initially cooling the grain-oriented $YBa_2Cu_3O_7$ sample down to 4.2 K in zero field. An external field $\mathbf{H}_e$ was then applied at a fixed angle θ_e relative to the *a-b* plane and its magnitude increased in stages up to 14 kOe. At each stage, the longitudinal and transverse components (M_L,M_T) of the total sample magnetization were measured, and the data were inserted into Eqs. (2) and (3) in order to calculate the components along *a-b* and *c* of the internal (demagnetization-corrected) field $\mathbf{H}$ and of the penetrating (vortex-flux) magnetization $\mathbf{M}_P$. Although these symmetry components are interesting separately, as shown later, we first combined them to obtain the vector moduli of $\mathbf{H}$ and $\mathbf{M}_P$ and their respective orientational angles, θ_H and θ_P, relative to *a-b*.

Figure 2 displays our results for H, M_P, θ_H, and θ_P as functions of H_e for different values of θ_e. We note that M_P rises from zero at H_e ranging from ~0.4 kOe for $\theta_e=30°$ to ~0.9 kOe for $\theta_e=75°$, corresponding, respectively, to H of ~0.5 and ~1.7 kOe, which give the range of the lower critical field H_{c1}. For fields below H_{c1}, it follows from Eq. (1) together with $M_{ab}=-\chi_0H_{ab}$ and $M_c=-\chi_0H_c$ that θ_H and θ_e, the orientational angles of $\mathbf{H}$ and $\mathbf{H}_e$, are related linearly through their tangents, i.e.,

$$\tan\theta_H=\alpha\tan\theta_3 , \quad \alpha=(1-\chi_0D_{ab})/(1-\chi_0D_c) , \tag{4}$$

which indicates, as expected, that θ_H differs from θ_e to the extent that D_{ab} differs from D_c. For our sample, $D_{ab}=3.364$, $D_c=5.838$, and $\chi_0=1/4\pi$, which give $\alpha=1.368$. Thus, for the set angles, $\theta_e=30°$, 45°, 60°, and 75°, Eq. (4) yields $\theta_H=38.3°$, 53.8°, 67.1°, and 78.9°, respectively. Figure 2(b) shows that θ_H starts at these values at low H_e, rises slightly, and then gradually diminishes and approaches θ_e as H_e increases and overcomes the anisotropy of the demagnetization.

In contrast to the variations of θ_H with H_e, we see in Fig. 2(b) that in each case θ_p, the orientational angle of the vortex-flux magnetization $\mathbf{M}_P$, starts with a small value and then rises and approaches θ_e with increasing H_e. Thus, at fields just above H_{c1}, $\mathbf{M}_P$ first appears at an orientation much closer to the a-b plane, compared to the orientation of $\mathbf{H}$. This initial preferential orientation of $\mathbf{M}_P$ persists (with $\theta_P \approx 30°$) even when θ_H is nearly 80° (in the case of $\theta_e = 75°$).

At this point it may be clarifying to see vectorially how our results emerge from the original data. The vector diagram of Fig. 3 illustrates the case of $\theta_e = 45°$ for $H_e = 2$, 6, and 10 kOe. The total sample magnetization $\mathbf{M}$, determined from its measured components relative to $\mathbf{H}_e$, is shown to be oriented diamagnetically at a small angle relative to the c axis. Using $\mathbf{M}$ we evaluated the anisotropic demagnetization and corrected $\mathbf{H}_e$ to obtain the internal field $\mathbf{H}$. Note that $\mathbf{H}$ is turned from $\mathbf{H}_e$ toward the direction of $-\mathbf{M}$ with an increase in size. We then determined

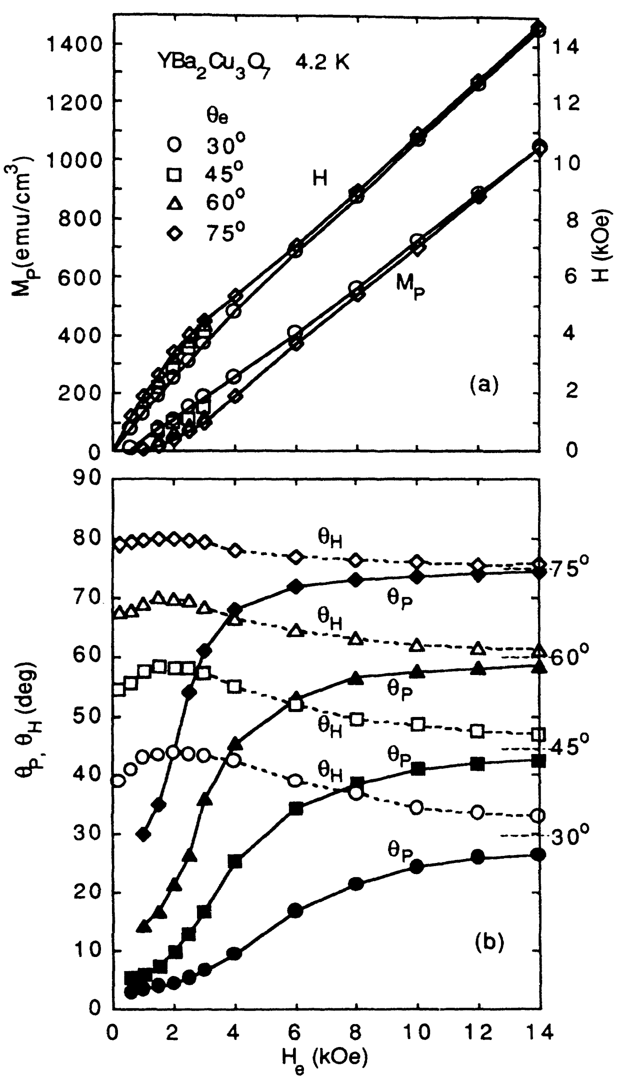

FIG. 2. (a) The magnitudes of $\mathbf{M}_P$ and $\mathbf{H}$ and (b) θ_P and θ_H, their orientational angles relative to a-b, as functions of increasing H_e at various angles θ_e relative to a-b after zero-field cooling to 4.2 K.

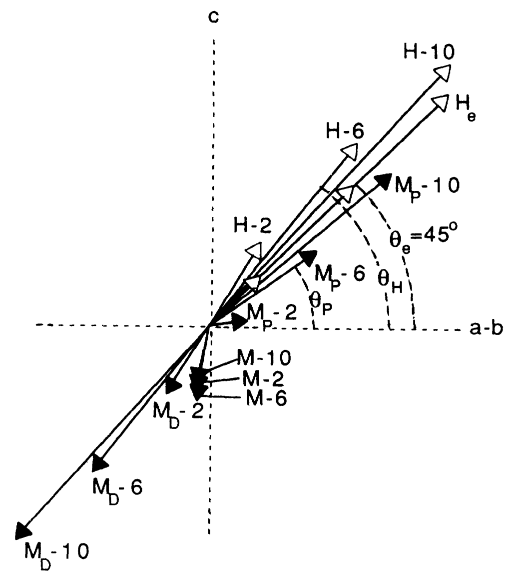

FIG. 3. Vectorial picture of sample magnetization $\mathbf{M}$, its vortex-flux and diamagnetic components $\mathbf{M}_P$ and $\mathbf{M}_D$, and the internal field $\mathbf{H}$, at $H_e = 2$, 6, and 10 kOe and $\theta_e = 45°$. θ_P and θ_H, orientational angles of $\mathbf{M}_P$ and $\mathbf{H}$ relative to a-b are indicated for $H_e = 6$ kOe.

$\mathbf{M}_D = -\mathbf{H}/4\pi$, the screening component of $\mathbf{M}$, and subtracted it vectorially from $\mathbf{M}$ to find $\mathbf{M}_P$, the penetrating vortex-flux component. At $H_e = 2$ kOe, $\mathbf{M}_P$ is seen to be quite small and oriented close to a-b. At higher H_e, $\mathbf{M}_P$ grows rapidly and turns toward $\mathbf{H}_e$, such that $\mathbf{M}_P$ and $\mathbf{M}_D$ are both large and nearly antiparallel to each other, with $\mathbf{M}$ representing their small vector sum. Indeed, the relatively constant size and direction of $\mathbf{M}$ is a coincidence of much less importance than the changes of $\mathbf{M}_P$. Note that Fig. 3 differs in aspect from Fig. 1, in which $\mathbf{M}$ was taken schematically to have a positive projection on $\mathbf{H}_e$.

From the results plotted in Fig. 2 and illustrated vectorially in Fig. 3, we have seen that for fields applied in various directions after zero-field cooling, the vortex-flux magnetization $\mathbf{M}_P$ is consistently oriented toward the a-b plane. A strong preference of $\mathbf{M}_P$ for the a-b plane can also be deduced indirectly from the initial magnetization curves for $\mathbf{H}$ along a-b and along c. These curves for our grain-oriented sample measured after zero-field cooling to 4.2 K are shown in Fig. 4(a), where the total magnetization M is plotted versus the demagnetization-corrected field H. Since at any H the diamagnetic screening component M_D is the same ($= -H/4\pi$) for both curves, the separation between them in M corresponds to a difference in the penetrating vortex-flux component M_P. To concentrate on the latter component we subtracted $-H/4\pi$ from the measured M at each H, and the resulting M_P versus H curves are shown in Fig. 4(b). These curves clearly testify that the penetration of vortex flux for H above H_{c1} occurs much more readily in the a-b plane than along the c axis, and this difference can be ascribed to the stronger pinning forces on the vortex lines along c.

The M_P versus H curves of Fig. 4(b) were therefore

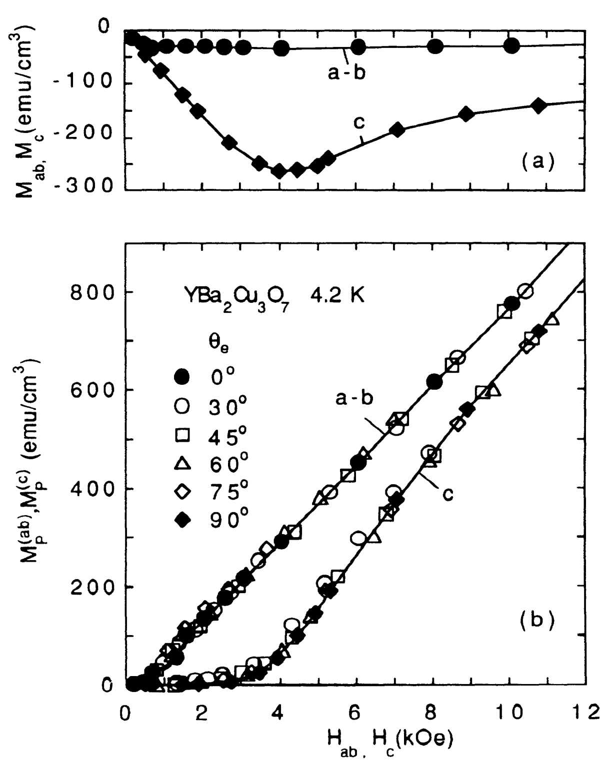

FIG. 4. (a) Total magnetization M versus internal field H for **H** along a-b ($\theta_e=0°$) or along c ($\theta_e=90°$). (b) Vortex-flux magnetization components, $M_P^{(ab)}$ and $M_P^{(c)}$, plotted, respectively, versus internal field components, H_{ab} and H_c, for different values of θ_e. In all cases, H is increasing after zero-field cooling to 4.2 K.

used as references for our results displayed in Fig. 2. For this comparison, the latter results for $\mathbf{M}_P$ and **H** for various θ_e were converted back into their components along a-b and c and then plotted, respectively, against each other in Fig. 4(b). The remarkable outcome, as we see, is that all the plotted points fall very close to the corresponding curves for **H** along a-b and c (i.e., for $\theta_e=0°$ and 90°). From the essential universality of these two curves, it appears that starting from the zero-field cooled state the production of vortex flux along a-b and its production along c are governed independently by the field components in these directions and by very different pinning forces. Indeed, the scaling of our results suggests that the vortex lines are all aligned along one or both of the two symmetry directions and do not assume some composite path. This situation contrasts with that of the cross-flux effect in the same grain-oriented sample,[7] in which trapped flux along c inhibits the subsequent production of vortex flux by fields in the a-b plane.

In the present work we also studied the trapped flux that is retained after the external field $\mathbf{H}_e$ applied in different directions is reduced from the maximum value (14 kOe) to zero. Figure 2 shows that at the maximum H_e the directions of $\mathbf{M}_P$ and **H** are both very close to that of $\mathbf{H}_e$, which are the starting conditions for the formation of an isothermal remanence $\mathbf{M}_R$ corresponding to the trapped vortex flux. Our results for $\mathbf{M}_R$ are displayed in Fig. 5, where (a) shows θ_R, the orientational angle of $\mathbf{M}_R$ relative to a-b, plotted against θ_e, the corresponding angle for $\mathbf{H}_e$. Clearly, except for the end points at 0° and 90°, θ_R is consistently larger than θ_e, indicating that $\mathbf{M}_R$ has a distinct orientational preference for the c axis. Although this reference is not so extreme as that reported from earlier work[4] (which has $\mathbf{M}_R$ essentially parallel to c for various θ_e), it does contrast sharply with our θ_P versus θ_H results for the initial vortex-flux magnetization $\mathbf{M}_P$ after zero-field cooling. The latter results, taken from Fig. 2, are also plotted in Fig. 5(a), where the preference of the initial $\mathbf{M}_P$ for the a-b plane is very evident. However, this contrast in behavior is not conflicting; on the contrary, it represents two different manifestations of the stronger pinning for the vortex lines along c than for those along a-b.

Nevertheless, our results for the trapped-flux magnetization $\mathbf{M}_R$ have some anomalous features. In Fig. 5(b) the components of $\mathbf{M}_R$ along a-b and along c are plotted versus θ_e. Although $M_R^{(c)}$ varies monotonically with θ_e as

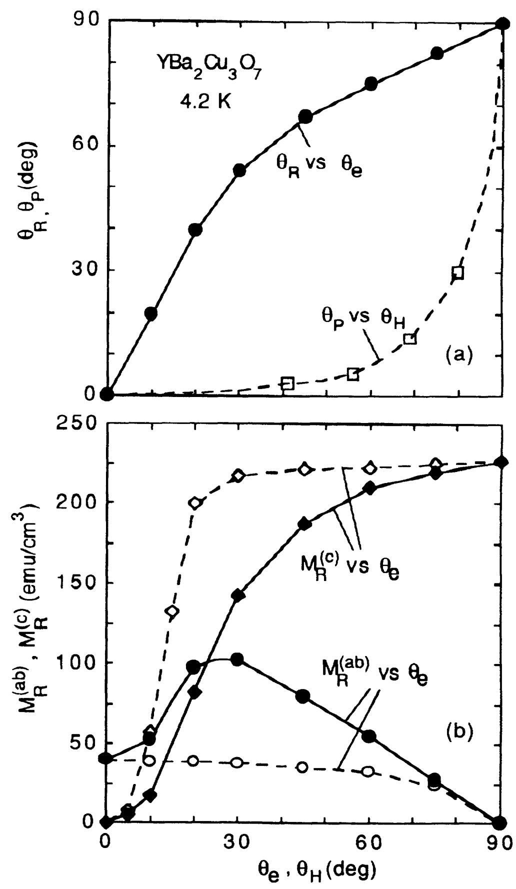

FIG. 5. (a) θ_R, orientational angle of remanent trapped-flux magnetization $\mathbf{M}_R$, versus θ_e, orientational angle of external field $\mathbf{H}_e$ (=14 kOe before removal); θ_P initial orientational angle of vortex-flux magnetization, versus θ_H, corresponding angle of internal field after zero-field cooling. (b) Components of $\mathbf{M}_R$ along a-b and c versus θ_e; solid curves are through measured values and dashed curves are through values derived from curves in Fig. 6, as described in text. All angles are with reference to a-b plane.

expected, we see that $M_R^{(ab)}$ goes through a broad but pronounced maximum. This peculiar behavior, as we will show, eliminates the possibility of any scaling analogous to that in Fig. 4 for the components of $\mathbf{M}_P$ with increasing field. To investigate this possibility, we make use of the curves shown in Fig. 6 for the isothermal remanence M_R at 4.2 K as a function of the external field H_e that is applied along *a-b* or *c* and then removed. We consider that for $\mathbf{H}_e$ of 14 kOe applied in some arbitrary direction (and removed), its components along *a-b* and *c* will produce the components of $\mathbf{M}_R$ taken, respectively, from these curves. The results of this exercise are shown as dashed curves in Fig. 5(b), where they can be compared with the solid curves for the quantities measured directly. It is clear that the dashed $M_R^{(ab)}$ versus θ_e curve lies consistently lower (with no maximum) while the dashed $M_R^{(c)}$ versus θ_e curve lies consistently higher than the corresponding solid curves (except, of course, at $\theta_e = 0°$ and $90°$). Thus, the trapped flux measured directly has a weaker orientational preference for the *c* axis than it would if it were produced separately by the field components along *a-b* and *c*. This discrepancy suggests that the trapped vortex lines are not aligned purely along *a-b* and along *c*. Instead, they probably alternate between these directions, as suggested recently on theoretical grounds.[8] In such a stepwise configuration, the strong pinning of the vortex *c* components would also be effective for the *a-b* components, thus reducing the apparent preference of $\mathbf{M}_R$ for the *c* axis. It is intriguing as to why such a configuration seems to pertain to the trapped vortex lines but not to the vortices that exist (at higher concentration) before the field is removed. Further experiments under different hysteretic conditions, plus an appropriate conceptual model, are needed for a detailed understanding of the various vortex structures in the CuO_2-layered compounds.

As we have shown, our results for the trapped-flux magnetization $\mathbf{M}_R$ in $YBa_2Cu_3O_7$ indicate a considerably weaker preference of $\mathbf{M}_R$ for the *c* axis than the results reported in Ref. 4. In a very recent comment, Ref. 9, it is pointed out that the latter results are strongly affected by the highly anisotropic demagnetization of the single-crystal sample. In the authors' reply, Ref. 10, it is claimed that this effect, though strong, does not totally mask an intrinsic preference of $\mathbf{M}_R$ for the *c* axis. Hence, the discrepancy with our results for a grain-oriented sample, where the demagnetization is much less anisotropic, appears to be reduced, if not eliminated.

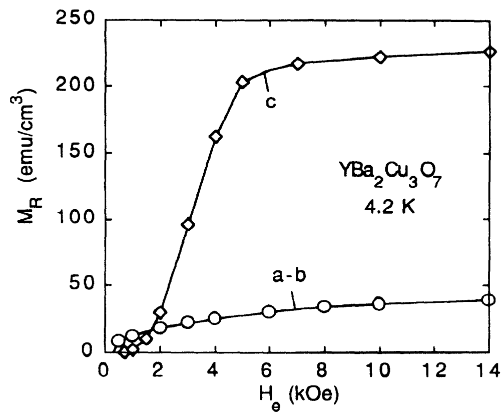

FIG. 6. Remanent trapped-flux magnetization M_R versus external field H_e for $\mathbf{H}_e$ applied along *a-b* or *c* and then removed, after zero-field cooling to 4.2 K.

ACKNOWLEDGMENTS

We are grateful to Mohana Yethiraj for the preparation of the grain-oriented material at LANL. The work at UIC was supported in part by the National Science Foundation under Grant No. DMR-87-22880.

[1]L. J. Campbell, M. M. Doria, and V. G. Kogan, Phys. Rev. B **38**, 2439 (1988); V. G. Kogan and L. J. Campbell, Phys. Rev. Lett. **62**, 1552 (1989).

[2]G. J. Dolan, G. V. Chandrashekhar, T. R. Dinger, C. Feild, and F. Holtzberg, Phys. Rev. Lett. **62**, 827 (1989); G. J. Dolan, F. Holtzberg, C Feild, and T. R. Dinger, *ibid.* **62**, 2184 (1989).

[3]M. Tachiki and S. Takahashi, Physica C **162-164**, 241 (1989).

[4]I. Felner, U. Yaron, Y. Yeshurun, G. V. Chandrashekhar, and F. Holtzberg, Physica C **162-164**, 1635 (1989); Phys. Rev. B **40**, 5239 (1989).

[5]Liwen Liu, J. S. Kouvel, and T. O. Brun, Phys. Rev. B **38**, 11 799 (1988); J. Phys. (Paris) **49**, C8-2189 (1988).

[6]Liwen Liu, J. S. Kouvel, and T. O. Brun, J. Appl. Phys. **67**, 4527 (1990); Phys. Rev. B **43**, 7859 (1991).

[7]Liwen Liu, J. S. Kouvel, and T. O. Brun, Phys. Rev. B **43**, 11 481 (1991).

[8]S. Doniach, in *The Los Alamos Symposium—1989 High Temperature Superconductivity Proceedings,* edited by K. S. Bedell *et al.* (Addison-Wesley, New York, 1990), p. 406.

[9]S. Kolesnik, T. Skoskiewicz, and J. Igalson, Phys. Rev. B **43**, 13 679 (1991).

[10]I. Felner, U. Yaron, and Y. Yeshurun, Phys. Rev. B **43**, 13 681 (1991).